Miner Petrol (2009) 95:273–290
DOI 10.1007/s00710-009-0044-7

ORIGINAL PAPER

Hydrous aluminosilicate metasomatism in an intra-oceanic subduction zone: Implications from the Kurancali (Turkey) ultramafic-mafic cumulates within the Alpine Neotethys Ocean

Fatma Toksoy-Köksal · Roland Oberhaensli · M. Cemal Göncüoglu

Received: 30 March 2008 / Accepted: 21 January 2009 / Published online: 18 February 2009

Abstract The Kurancali ultramafic-mafic cumulate body, an allochthonous ophiolitic sliver in central Anatolia, is characterized by the presence of abundant hydrous phases (phlogopite, pargasite) besides augitic diopside, plagioclase, and accessory amounts of rutile, sphene, apatite, zircon, and calcite. Based on modes of the essential minerals, the olivine-orthopyroxene-free cumulates are grouped as clinopyroxenite, hydrous clinopyroxenite, phlogopitite, hornblendite, layered gabbro, and diorite. Petrographical, mineralogical and geochemical features of the rocks infer crystallization from a hydrous magma having high-K calc-alkaline affinity with slightly alkaline character, and point to metasomatised mantle as the magma source. Our evidence implies that the metasomatising component, which modified the composition of the mantle wedge source rock in an intra-oceanic subduction zone, was a H_2O, alkali and carbonate-rich aluminosilicate fluid and/or melt, probably derived from a subducted slab. We suggest that the metasomatic agents in the subarc mantle led to the generation of a hydrous magma, which produced the Kurancali cumulates in an island-arc basement in a supra-subduction-zone setting during the closure of the Izmir-Ankara-Erzincan branch of the Alpine Neotethys Ocean.

Analyses were made at GeoForschungsZentrum Potsdam (GFZ) and Institut für Geowissenschaften, Universität Potsdam, Germany

Editorial handling: H. Marschall

F. Toksoy-Köksal (✉) · M. C. Göncüoglu
Department of Geological Engineering,
Middle East Technical University,
06531 Ankara, Turkey
e-mail: ftkoksal@metu.edu.tr

M. C. Göncüoglu
e-mail: mcgoncu@metu.edu.tr

R. Oberhaensli
Department of Geosciences, University of Potsdam,
Potsdam, Germany
e-mail: Roland.Oberhaensli@geo.uni-potsdam.de

Introduction

Generation and composition of calc-alkaline magmas beneath an arc in subduction zones are controlled by numerous reservoirs comprising variably depleted and metasomatised peridotitic mantle wedge materials. In general, these magmas are distinguished by excessive enrichment in large ion lithophile elements (LILE) and light rare earth elements (LREE), causing higher LILE/HFSE and LREE/HFSE ratios compared to typical of mantle-derived melts, although they are also slightly enriched in high field-strength elements (HFSE) (e.g., Pearce et al. 1999; Zanetti et al. 1999; Green and Sinha 2005). Mantle metasomatism by influx of subduction-derived components is the essential event resulting in variably enriched mantle wedge materials that will produce arc magmas (e.g., Pearce and Peate 1995; Yu et al. 2006). Moreover, metasomatising agents are highly variable as CO_2-, H_2O-, halogen- or P-rich fluids (e.g., Gorring and Kay 2000), Fe-Ti-K-rich basaltic melts (e.g., Menzies et al. 1987), adakitic melts (e.g., Defant and Drummond 1990; Kepezhinskas et al. 1995; Yogodzinski et al. 1995; Coltorti et al. 2007), siliceous melts (e.g., Elliott 2003; Green and Sinha 2005), hydrous siliceous melts (e.g., Pearce et al. 1999; McInnes et al. 2001), volatile-rich, alkaline aluminosilicate melts (e.g., Kepezhinskas et al. 1995), carbonatitic melts (e.g., Gorring and Kay 2000; Coltorti et al. 2007), and melilitic or melanephelinitic melts (e.g., Chalot-Prat and Boullier 1997). Type of metasomatic agent and degree of

metasomatism may lead to distinct chemical variations in mantle wedge material and so in their melting products. For instance, high-density, H_2O-rich fluid with dissolved components (alkali aluminosilicate melt and aqueous carbon and sulphur species) derived from dehydration of subducted, altered oceanic crust can metasomatise mantle peridotite to enrich it in orthopyroxene, clinopyroxene, phlogopite, amphibole, magnetite, and Fe-Ni sulphides (e.g., McInnes et al. 2001). Partial melting of a metasomatically enriched mantle wedge source can produce a hydrous alkali-rich calc-alkaline magma in island arc environments (e.g., McInnes et al. 2001), and crystallization of such a magma may lead to enrichment in hydrous minerals (phlogopite and pargasite).

A cumulate body, extremely abundant in phlogopite and pargasite is exposed as a tectonic sliver in the Kurancali area, central Anatolia. This hydrous cumulate body is the representative of an island arc basement formed during the closure of the Neotethyan Ocean (Toksoy-Köksal 2003) and may contribute to better-understanding of the processes and products of mantle metasomatism in an intra-oceanic subduction zone. We studied these rocks by the aid of detailed whole-rock and mineral chemical analyses to dechipher the compositional effects imparted to mantle lithosphere by subduction-derived components in a compressional environment. The main points to be addressed are; (1) which kind of metasomatic processes pervasively enriched the source in incompatible elements, and resulted in SiO_2 undersaturation, and Al_2O_3-CaO-alkali-TiO_2 enrichment in melt derived from this source, (2) the origin and composition of the metasomatic agent(s).

Regional geological setting

The Neotethys Ocean, opened during fragmentation of northern Gondwana, was largely consumed by convergence of Africa and Eurasia during the Late Cretaceous (e.g., Sengör and Yilmaz 1981). The Turkish sector of the Neotethyan suture is characterized by two major east-west trending belts of variably disrupted fragments of ophiolites (Sengör and Yilmaz 1981). Each belt records closure and destruction of a separate branch of the Neotethyan ocean: (a) the northern branch located at north of the Tauride-Anatolide Platform (TAP) comprises the Izmir-Ankara-Erzincan (IAE) and Intra-Pontide oceans, and (b) the southern branch is represented by well documented ophiolite bodies (e.g., Troodos, Hatay, Guleman and Cilo) between the Arabian Platform and the TAP (e.g., Göncüoglu et al. 1997).

The IAE ocean of the northern Neotethys reached its maximum size during the Early Cretaceous, and was consumed by northward subduction, giving rise to obduction of ophiolites towards south onto the passive margin of the TAP during Late Cretaceous (e.g., Sengör and Yilmaz 1981; Göncüoglu et al. 1997). Allochthonous bodies of subduction-influenced mafic and ultramafic rocks in central Anatolia (Turkey) are described as supra-subduction type ophiolites (e.g., Türeli et al. 1993; Yaliniz et al. 1996, 2000; Floyd et al. 2000; Toksoy-Köksal 2003; Toksoy-Köksal et al. 2001a; Kocak et al. 2005), i.e., the Central Anatolian Ophiolites (CAO; Göncüoglu et al. 1991). CAO include the meta-ophiolites and sub-ophiolitic metamorphics. These ophiolitic units display remarkable differences in their geochemical characteristics suggesting variations in source area and tectonic settings within an intra-oceanic subduction zone, such as fore-arc (e.g., Yaliniz et al. 2000), back-arc (e.g., Floyd et al. 2000) or island-arc (e.g., Toksoy-Köksal 2003).

In central Turkey, the passive margin of the TAP, on which ophiolitic fragments were obducted, is represented by the Central Anatolian Crystalline Complex (CACC), an assemblage of magmatic and metamorphic rocks. It includes the Central Anatolian Metamorphics (CAM), Central Anatolian Granitoids (CAG) besides CAO (Fig. 1) (e.g., Göncüoglu et al. 1991). The CAM consists of polyphase metamorphic platform sequences. A metamorphic ophiolite-bearing mélange developed during the emplacement of the CAO onto the CAM appears in the uppermost part of the CAM. The main metamorphism and ophiolite emplacement in the CACC occurred during late Cenomanian (Göncüoglu 1986) or post-Cenomanian (Whitney et al. 2003; U-Pb SHRIMP zircon age of 91±2 Ma) times. The CAG intrudes both the CAM and the CAO units.

Allochthonous dismembered and scattered ophiolitic bodies shown on Fig. 1 consistently display thrust contacts with the CAM with thin tectonic slivers of sub-ophiolitic amphibolites locally occurring in the thrust zone. The ophiolitic bodies, having a partially preserved magmatic pseudostratigraphy, include serpentinized ultramafic rocks, layered and isotropic gabbros, plagiogranite, dolerite dykes, basaltic volcanic sequence (pillow basalts, massive lava flows), and late dykes cutting the lavas and sedimentary cover. In addition to these, many isolated bodies of ultramafic and massive/layered gabbroic rocks are found as tectonic slivers (e.g., Yaliniz and Göncüoglu 1998).

Among the isolated ophiolitic bodies, the Kurancali ultramafic-mafic cumulate body from east of Kaman has reserved a specific interest by its mineralogical and geochemical properties (e.g., Toksoy-Köksal 2003; Toksoy-Köksal et al. 2001a, 2007).

Geology

The Kurancali area is a critical location to study the contact relationships of the CAO rocks and the main units of the CAM (Toksoy 1998; Toksoy-Köksal 2003). In this area, the lower units of the CAO (i.e., ultramafic-mafic cumulates)

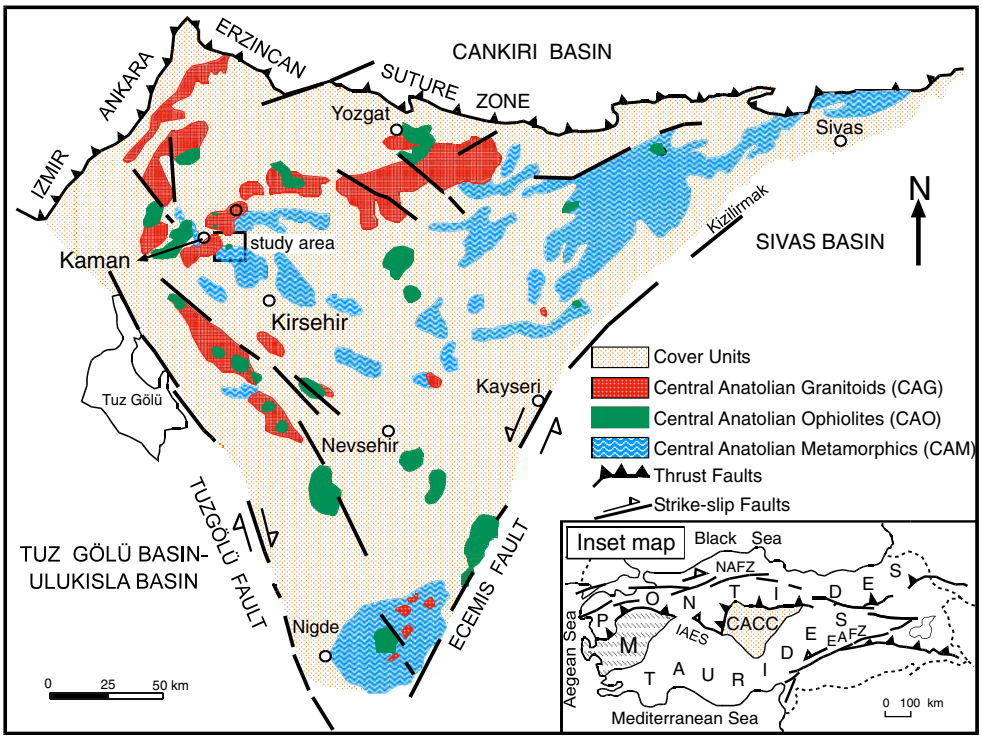

Fig. 1 Simplified geological map of central Anatolia (In inset map: CACC: Central Anatolian Crystalline Complex, M: Menderes Massif, NAFZ: North Anatolian Faults Zone, EAFZ: East Anatolian Fault Zone, IAES: Izmir-Ankara-Erzincan Suture) (from Göncüoglu et al. 1991)

rest on the amphibolites and calc-silicate amphibolites of the metamorphic ophiolitic mélange of the CAM (Fig. 2). Detailed field-observations reveals that the cumulates along the contact are characterized by foliated amphibolites and amphibole-pyroxene gneisses. Moreover, elongated boudins of cumulates, amphibolites and serpentinites are observed within a sheared zone above the mélange.

The Kurancali ultramafic-mafic cumulate body is represented by a 1,500 m long and 1,000 m wide tectonic sliver (Fig. 2). It mainly comprises layered gabbro with an alternation of diorite, clinopyroxenite, hydrous clinopyroxenite, phlogopitite and hornblendite (Fig. 2). The rock units are a few tens of cm to 3–4 m in thickness and can only be followed a few tens of meters along-strike. So, only the main rock types are shown on the map (Fig. 2). The underlying metamorphic ophiolitic mélange, represented by blocks of meta-ophiolitic rocks and meta-carbonates, is prevailed by irregular bands and lenses of calc-silicate amphibolites, calc-silicate marbles, cherty marbles, amphibolites and serpentinites within a foliated matrix. Matrix of the mélange is dominated by calc-silicate biotite-gneisses and amphibole-biotite-gneisses. The amount of calc-silicate rocks diminishes while amphibole-biotite-gneisses increases away from the underlying meta-carbonate contact. All units (metamorphic ophiolitic mélange, shear zone and ultramafic-mafic cumulate rock sliver) are cut by NW-SE trending granitoid dykes with sharp contacts with their host rocks. They are made up of K-feldspar granite, quartz syenite and syenite with varying crystal size from 0.5 mm to 4 mm. The dykes are representatives of the CAG, with intrusion ages varying between 85 and 71 Ma (e.g., Köksal et al. 2004; Boztug et al. 2007; Köksal and Göncüoglu 2008). Detailed studies on this unique tectonic sliver revealed the presence of cumulate ultramafics, layered gabbros and diorites (e.g., Toksoy-Köksal 2003; Toksoy-Köksal et al. 2007). In previous studies, this cumulate body was referred to as the Kurancali meta-ophiolitic peridotite (Yaliniz and Göncüoglu 1998) or as the Kurancali meta-gabbro (e.g., Toksoy 1998; Toksoy-Köksal et al. 2001a,b).

Petrography

Petrographical studies exhibit that the Kurancali ultramafic-mafic body is distinct due to the presence of abundant phlogopitic mica and pargasitic amphibole. Besides hydrous minerals, clinopyroxene and plagioclase are present in these rocks. The rocks are typically free of olivine and orthopyroxene. They show heterogeneity in both composition (leuco to melano) and grain size (fine-grained to pegmatitic). They are characterized by their well-preserved cumulate texture (Fig. 3), and crystallization order of the phases is clinopyroxene, phlogopite, pargasite and plagioclase. The first three minerals are cumulate phases while the last one is an intercumulate phase. Orthocumulate texture dominates in clinopyroxenite and phlogopitite but adcumulate texture appears in hydrous clinopyroxenite, hornblendite, layered gabbro and diorite.

The main rock types and their modal composition are given in Table 1. Clinopyroxenite consists mainly of

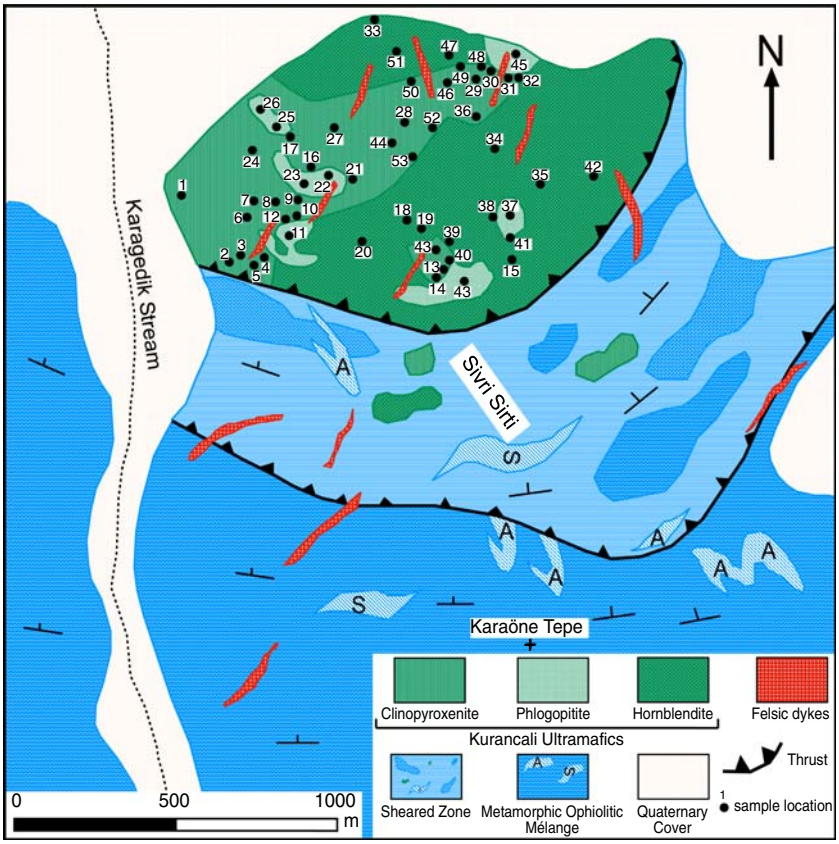

Fig. 2 Geological map of the study area (Toksoy 1998)

clinopyroxene. Coarse grained phlogopite also appears in this rock, where it occurs close to phlogopitite. Plagioclase and pargasite I are absent in clinopyroxenite. However, hydrous clinopyroxenite has variable amounts of fine- to coarse-grained plagioclase, pargasite II and phlogopite as well as clinopyroxene. This rock type is found close to the phlogopitite and hornblendite where amphibole+plagioclase pods are common. Irregular masses of pegmatitic phlogopitite consist mainly of phlogopite phenocryts, enclosing minor amounts of clinopyroxene. Almost no plagioclase is present in phlogopitite. The presence of pargasite II in phlogopitite is restricted to where it is in contact to hornblendite, and generally found in small amphibole-plagioclase veins. Hornblendite is mainly composed of black pargasite I with minor amounts of plagioclase. Based on crystal size, it is divided into two groups as fine-grained and pegmatitic hornblendites. Fine-grained hornblendite contains very limited amounts of plagioclase and clinopyroxene (less than 5%), while pegmatitic hornblendite contains up to 15% plagioclase, but lacks clinopyroxene. A few tiny relict crystals of clinopyroxene and phlogopite were identified in crystals of pargasite I in pegmatitic

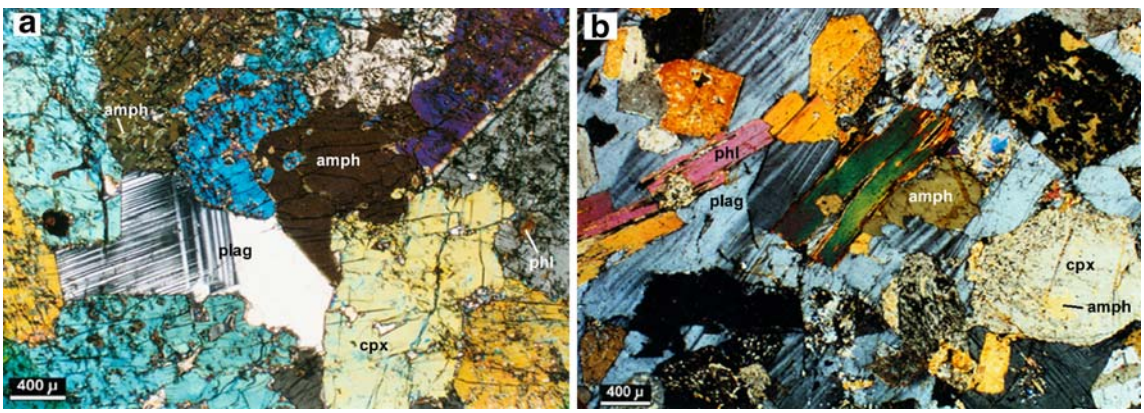

Fig. 3 Photomicrographs showing **a** orthocumulate texture from a clinopyroxenite sample, **b** adcumulate texture from hydrous clinopyroxenite samples where plagioclase is intercumulus phase (analyzer in position)

Table 1 Modal abundances of major minerals in the rocks

Rock Mineral	clinopyroxenite	phlogopitite	hydrous clinopyroxenite	hornblendite (fine grained)	hornblendite (coarse grained)	layered gabbro	diorite
diopsidic augite	>90	~15	~55	3–4	0.5–1	~50	<3
phlogopite	~5	~80	~15	<1	~5	~5	~62
pargasite	~3	~3	~10	>90	>85	~5	–
plagioclase	~3–4	~3–4	~20	~5	5–10 (~80*)	~40	~35

*in leucocratic parts of hornblendite

hornblendite. In pegmatitic hornblendite, plagioclase is generally found as aggregates forming leucocratic parts, probably formed by strong magmatic filter pressing. Layered gabbro with varying grain sizes between 3–5 mm and 1–1.5 cm is marked by variations of modal proportions of (mainly) clinopyroxene to plagioclase. In coarser-grained domains, amphibole and plagioclase are present. These domains may represent re-injection of plagioclase +amphibole-precipitating liquids into clinopyroxene +plagioclase layers. This is inferred from the pothole-like structures and layers filled by coarse-grained amphibole and plagioclase within layered gabbro and hydrous clinopyroxenite. Moreover, small veins of plagioclase+amphibole in clinopyroxenite, hydrous clinopyroxenite and phlogopitite also support this idea. Diorite contains dominantly light brownish phlogopite and plagioclase. It shows a rather homogeneous mineral and grain-size distribution.

Clinopyroxene is the most abundant mineral (Table 1), found in variable amounts and sizes from a few mm to pegmatitic (up to 2.0 cm). It is rarely zoned and shows a diopsidic-augite composition. In cataclastically fragmented parts, crystals are commonly replaced by late magmatic amphibole and mica at rims and along cleavage and fracture planes, resulting in a spongy appearance.

Euhedral to subhedral crystals of phlogopite with variable grain sizes (few mm to 2–2.5 cm) show a dark brownish colour and strong pleochroism. Kink banding, due to syn-magmatic deformation is a common feature. In general, the crystals are fresh except for a limited degree of alteration to vermiculite and chlorite in places (e.g., Toksoy-Köksal et al. 2001b).

Both primary and late-magmatic amphiboles are pargasitic in composition. Primary magmatic pargasite (pargasite I) is found in variable sizes with up to euhedral 20 cm long prisms. Late magmatic pargasite (pargasite II) occurs either as pseudomorphs after clinopyroxene (pargasite IIa), or as overgrowth on clinopyroxene crystals and interstitials between them (pargasite IIb). Pargasite IIa is probably due to reaction between a melt (residual or infiltrating) and clinopyroxene. In general, pargasite I and IIa are not found in association with phlogopite, while the pargasite IIb coexists with phlogopite, especially in layered gabbros and in amphibole-plagioclase-rich veins. Pargasite I shows strong pleochroism between various shades of brown, and rarely shows faint optical zoning and twinning. The pargasite IIa is brownish green, while the pargasite IIb are green.

Plagioclase is present in almost all rock types in variable amounts (Table 1). Crystals are anhedral to subhedral and rarely show weak zoning.

Accessory minerals are Ti-rich phases, apatite, zircon and pyrite. Sphene with strong pleochroism is the most common Ti-phase, found either as post-cumulus phase or as small inclusions in clinopyroxene. Blackish tiny needle-like crystals of rutile are found as aggregates in pargasite I and clinopyroxene. Small ilmenite crystals at boundaries of phlogopites, sporadic apatite aggregates and pyrite rarely occur. Zircon crystals were too tiny to be petrographically identified. Rare calcite, vermiculite (Toksoy 1998; Toksoy-Köksal et al. 2001b) and sericite as surface alteration products, and actinolite, chlorite, pumpellite, epidote as low-grade metamorphic phases are also present in the rocks.

Geochemical results

Analytical methods

Whole-rock geochemical analyses were performed for 52 samples. All of the samples were analysed for major, minor and selected trace elements (Ba, Cr, Ni, Rb, Sr, V, Y, Zn, Zr) by Bruker-axs SRS303-AS XRF with a Rh X-ray tube at standard running conditions at GeoForschungsZentrum Potsdam (GFZ), Germany. For these samples, ferrous iron by $K_2Cr_2O_7$ titration, and CO_2, H_2O^+ using Vario EL were measured at Institut für Geowissenschaften, Universität Potsdam. For 17 representative samples, some trace elements including Sc, Co, Cu, Ga, Nb, Cd, Sn, Cs, Ta, Pb, Th, U, were measured by a VG Elemental Plasma Quad System PQ2+ ICP-MS in GFZ. Rare earth element (REE) analyses of these samples were carried out using a Scanni VARIAN Vista MPX ICP-AES at Institut für Geowissenschaften, Universität Potsdam. Five additional samples were analysed by ICP-MS and ICP-OES at ACME laboratories (Canada) for the full range of elements, including Hf and Mo.

Approximately 1,700 point analyses of the rock-forming minerals of 21 rock samples were carried out by electron microprobe (EMP) at GFZ. The analyses were performed by a fully automated CAMECA SX-100 EMP. The instrument was operated in wavelength-dispersion mode, with the electron beam accelerated to 15 kV at 20 nA beam current. The applied beam (spot) size was 5 μm for clinopyroxene, amphibole and mica, and 10 μm for feldspar. A variety of natural and synthetic standards were used for calibration. Matrix corrections were performed by the PAP procedure in the CAMECA software.

Mineral chemistry

Compositional ranges for the minerals are compiled in Table 2 (the whole data set is available from the first author upon request). Conversion of oxides into cations, site allocations and classifications of clinopyroxene, mica and amphibole were done according to recommendations of the International Mineralogical Association (IMA) (Morimoto 1989; Rieder et al. 1998; Leake et al. 1997, respectively). Ferric and ferrous iron values for clinopyroxene and amphibole were derived based on the equation of Droop (1987), and for mica they were measured by applying $K_2Cr_2O_7$ titration method on mineral separates of eight samples. Formulae of plagioclase were calculated based on five cations, and cations are allocated to sites as Si, Al (sum of four) in tetrahedral site, Na, Ca, K and Ba (sum to one) in the large cation site.

Pyroxene

Clinopyroxene is diopside to diopsidic augite with a compositional range of $Wo_{44–52}En_{29–40}Fs_{11–23}$ where the Wo proportions above 50 are an artefact of high Al_2O_3, TiO_2 and Na_2O contents (0.37–8.66, 0.02–1.25, 0.10–0.97 wt%, respectively). Clinopyroxene with $Mg/(Mg+Fe^{2+})$ (Mg#) ranging from 0.59 to 0.88 shows compositional heterogeneity even within a single sample. Clinopyroxene shows an increase in Si, Fe^{2+} and Mn contents and a decrease in $Al^{(t)}$, Ca, Ti, Fe^{3+}, Mg, Na and K contents with decreasing Mg# from the ultramafic rocks to the mafic samples. Substitution mechanisms and Ti/Al ratios (1:5–1:20) infer that incorporation of Al into the crystal structure occurs as Ca-tschermaks molecule. Two distinct compositional trends, mainly based on Mg, Fe^{2+}, Ca and $Al^{[6]}$ contents, occur as a common feature of substitution mechanisms and variation diagrams (Toksoy-Köksal 2003) (e.g., Fig. 4a).

Dark mica

Mica with Mg#>0.5 is referred to as phlogopite although its composition departs from the ideal phlogopite/annite join, due to its high $Al^{[4]}$ (ca.2.5 pfu), Fe^{3+} (>0.31 pfu), Ti (>0.20 pfu) and $Al^{[6]}$ (0.01–0.56 pfu) contents, a substitutiton of F and Cl for OH, and the presence of vacancies in both octahedral and interlayer sites (see also Toksoy-Köksal 2003). Compositional changes in phlogopite are best explained by tschermakitic and coupled substitution mechanisms (Toksoy-Köksal 2003). Coupled mechanisms display the existence of excess mixing of Mg, Fe^{2+}, Fe^{3+}, Ti, $Al^{[6]}$ in octahedral site with vacancy, and exchange of K by Ba, Ca and Na in the interlayer site. It is characterized by an increase of Si, Ti, $Fe^{2+}$and Fe^{3+}, and a decrease of $Al^{[4]}$, $Al^{[6]}$, Mg and Na with decreasing Mg# in the sequence of phlogopitite - clinopyroxenite - hydrous clinopyroxenite - hornblendite - layered gabbro - diorite.

Amphibole

The majority of magmatic amphibole is pargasite in pegmatitic hornblendite, with subordinate ferro-pargasite. In contrast, fine-grained hornblendite contains magnesio-hastingsite. Pargasite I from pegmatitic hornblendite and pargasite II from clinopyroxenite, hydrous clinopyroxenite, phlogopitite and layered gabbro have Mg# (0.48–0.63), while magnesio-hastingsite in fine-grained hornblendite has higher Mg# (0.72–0.76) (Table 2). Pargasite and magnesio-hastingsite, which differ in Mg#, show compositional overlaps for Si, $Al^{(t)}$, Mn and Ca contents. Pargasite I and pargasite II do not show significant compositional variation. K and $Al^{(t)}$ contents of pargasite II from clinopyroxenite and phlogopitite are higher than those of other rocks, while their Ti contents are slightly lower. Both pargasite I and II are characterized by strong Al-tschermakite, Ti-tschermakite, edenite and pargasite substitutions, and weak Fe^{3+}-tschermakite substitution. Variations of Ca, Ti, Fe^{2+} and Mg contents against Mg# and exchange mechanisms are defined by two separate trends that are not related to texture, origin of amphibole or to rock type (Toksoy-Köksal 2003) (e.g., Fig. 4c).

Plagioclase

Plagioclase shows a wide range of An content (41–99%) even within single crystals. This variation is not controlled by rock type, texture or coexisting minerals (Toksoy-Köksal 2003). The substitution mechanisms are characterized by two different compositional trends for the samples even within the same rock (Fig. 4d).

Whole-rock geochemistry

The rocks are characterized by moderate Mg# (molecular ratio) (0.44–0.75) and low abundances of Cr (47–651 ppm), Ni (16–38 ppm) and Co (17–58 ppm). They present a wide range of compositions, controlled by modal compositions

Table 2 Ranges of electron microprobe analyses of the minerals. Whole data set is available upon request

Rocks Minerals	clinopyroxenite	phlogopitite	hydrous clinopyroxenite	hornblendite (fine grained)	hornblendite (coarse grained)	layered gabbro	diorite
Pyroxenes							
No. of analyses	*131*	*156*	*112*	*1*	*8*	*18*	*23*
SiO_2	45.59–52.88	48.38–53.71	46.27–52.61	52.4	50.20–53.53	50.89–53.16	50.98–52.73
TiO_2	0.02–1.13	0.01–0.89	0.08–1.16	0.14	0.05–0.45	0.04–0.60	0.07–0.49
Al_2O_3	0.43–8.64	0.72–6.41	0.72–8.66	1.32	0.36–4.65	0.39–3.64	0.40–2.23
$FeO^{(t)}$	6.12–12.45	6.91–12.62	8.67–11.89	9.34	7.35–11.34	9.39–11.02	12.09–14.17
MnO	0.08–0.34	0.15–0.46	0.19–0.43	0.29	0.21–0.40	0.31–0.39	0.38–0.54
MgO	8.77–14.28	9.72–13.99	9.71–13.04	12.7	11.56–13.67	11.85–12.92	10.41–11.20
CaO	22.30–25.76	22.06–24.99	19.20–24.78	24.3	21.97–24.69	22.71–23.85	21.86–23.15
Na_2O	0.10–0.86	0.18–0.80	0.15–0.97	0.31	0.13–0.35	0.15–0.37	0.13–0.31
K_2O	0.00–0.17	0.00–0.08	0.00–0.38	0.00	0.00–0.02	0.00–0.04	0.00–0.00
Cr_2O_3	0.00–0.12	0.00–0.12	0.00–0.06	0.00	0.00–0.05	0.00–0.06	0.00–0.03
NiO	0.00–0.07	0.00–0.09	0.00–0.08	0.00	0.00–0.07	0.00–0.10	0.00–0.00
Total	98.9–101.7	98.5–101.8	99.0–101.0	100.7	98.7–101.2	99.5–101.4	100.1–101.0
Micas							
No. of analyses	*38*	*65*	*142*		*24*	*15*	*95*
SiO_2	33.98–36.27	34.37–37.90	35.21–37.51		35.42–36.78	34.99–36.77	35.51–37.70
TiO_2	1.73–3.19	1.76–3.19	1.93–4.04		2.61–4.30	3.60–4.61	2.54–5.62
Al_2O_3	16.28–17.87	15.21–17.20	14.79–17.06		14.39–17.91	14.49–15.16	13.79–16.60
Cr_2O_3	0.00–0.05	0.00–0.12	0.00–0.05		0.00–0.05	0.00–0.06	0.00–0.05
$FeO^{(t)}$	16.50–21.97	12.68–20.85	15.67–20.99		17.41–21.34	17.79–19.93	18.63–22.08
MnO	0.09–0.21	0.08–0.24	0.09–0.26		0.10–0.20	0.07–0.16	0.07–0.22
MgO	10.38–13.80	12.80–17.56	10.25–14.27		9.98–13.25	11.20–12.39	8.59–11.22
CaO	0.00–0.21	0.00–0.35	0.00–0.65		0.00–2.86	0.00–0.12	0.00–0.41
Na_2O	0.08–0.33	0.07–0.46	0.06–0.28		0.08–0.30	0.06–0.18	0.07–0.20
K_2O	7.49–9.55	7.31–9.66	7.73–9.62		6.68–9.39	8.95–9.67	8.05–9.49
BaO	0.01–0.88	0.06–0.73	0.07–0.57		0.11–0.43	0.04–0.48	0.09–0.47
NiO	0.05–0.05	0.00–0.08	0.00–0.00		0.00–0.00	0.00–0.05	0.00–0.00
SrO	0.05–0.05	0.00–0.07	0.00–0.00		0.00–0.00	0.00–0.06	0.00–0.00
F	0.00–0.19	0.00–0.27	0.00–0.16		0.00–0.22	0.18–0.29	0.19–0.40
Cl	0.00–0.03	0.00–0.04	0.00–0.15		0.00–0.05	0.01–0.04	0.00–0.04
H_2O	3.77–3.99	3.82–4.05	3.82–4.02		3.81–4.00	3.75–3.86	3.69–3.87
True Total	93.5–96.6	94.2–96.9	94.3–97.5		94.6–96.8	94.2–96.8	94.1–97.7
Amphiboles							
No. of analyses	*85*	*121*	*81*	*21*	*93*	*12*	
SiO_2	38.40–40.57	38.80–41.60	38.36–41.44	39.19–41.86	37.69–42.29	39.63–40.93	
TiO_2	0.96–2.51	1.00–2.33	1.13–2.33	1.30–2.41	1.65–3.15	2.15–2.53	
Al_2O_3	13.53–16.27	12.52–16.14	12.93–16.31	12.72–15.14	12.70–15.24	14.02–14.98	
$FeO^{(t)}$	14.99–17.89	13.89–19.69	13.17–19.02	14.07–17.31	12.11–17.40	13.24–17.08	
MnO	0.12–0.29	0.15–0.36	0.16–0.34	0.15–0.29	0.14–0.31	0.21–0.25	
MgO	8.70–10.68	8.49–11.93	7.76–11.16	8.88–11.42	8.02–13.08	8.74–10.87	
CaO	10.82–12.75	11.27–12.55	10.47–12.42	11.87–12.47	10.79–12.11	11.89–12.10	
Na_2O	1.27–2.45	1.32–2.88	1.48–2.49	1.68–2.06	1.53–2.42	1.54–1.61	
K_2O	1.04–3.11	0.01–2.91	0.78–2.60	1.34–2.25	0.81–2.27	1.64–1.94	
Cr_2O_3	0.00–0.11	0.00–0.16	0.00–0.06	0.000–0.046	0.00–0.09	0.01–0.07	
NiO	0.000–0.098	0.000–0.084	0.000–0.044		0.000–0.067	0.000–0.049	
SrO	0.00–0.00	0.00–0.01	0.00–0.00		0.00–0.00	0.00–0.00	
F	0.00–0.16	0.000–0.204	0.00–0.07		0.00–0.16	0.06–0.14	
Cl	0.00–0.03	0.00–0.07			0.00–0.070	0.01–0.03	
True Total	96.6–99.3	96.7–99.4	96.8–99.2	97.8–99.3	95.3–99.5	96.5–98.5	
Plagioclases							
No. of analyses	*65*	*87*	*44*		*139*	*72*	*33*
SiO_2	44.16–56.25	46.49–56.98	45.94–56.75		43.70–56.25	44.03–57.93	46.18–58.45
TiO_2	0.00–0.03	0.00–0.05	0.00–0.04		0.00–0.05	0.00–0.04	0.26–0.26
Al_2O_3	28.03–35.52	27.25–34.96	27.69–35.12		28.03–35.29	27.16–35.31	26.29–34.21

Table 2 (continued)

Rocks Minerals	clinopyroxenite	phlogopitite	hydrous clinopyroxenite	hornblendite (fine grained)	hornblendite (coarse grained)	layered gabbro	diorite
MgO	0.00–0.04	0.00–0.02	0.00–0.01		0.00–0.04	0.00–0.25	0.00–0.87
CaO	8.95–19.59	9.64–18.26	8.61–18.49		9.66–19.00	8.96–19.21	8.36–18.58
MnO	0.00–0.05	0.00–0.05	0.00–0.07		0.00–0.04	0.00–0.04	0.00–0.09
$FeO^{(t)}$	0.01–0.42	0.02–0.22	0.02–0.82		0.01–0.42	0.00–0.41	0.04–0.57
BaO	0.00–0.07	0.00–0.10	0.00–0.08		0.00–0.06	0.00–0.05	0.00–0.06
Na_2O	0.43–5.98	1.44–6.18	0.90–6.11		0.75–5.98	0.77–6.47	1.06–6.75
K_2O	0.00–0.27	0.01–0.25	0.00–0.36		0.00–0.26	0.01–1.26	0.01–0.40
Total	98.1–101.3	98.8–101.4	98.4–101.2		95.6–101.3	98.2–100.9	99.1–101.4

of the samples (Table 3). Al_2O_3 contents decrease and CaO contents increase with increasing Mg#, due to highly variable modal proportions of plagioclase/diopsidic augite and pargasite/diopsidic augite.

N-MORB normalized (values from Sun and McDonough 1989) multi-element and REE patterns for all rock types are almost parallel to each other with only slight differences (Fig. 5) pointing to a petrogenetic relationship of the rocks. Marked differences are anomalies in Th, Nb, P, Zr, Ti and Eu, produced by strong control of these elements by the modal composition of the cumulates. The patterns, in general, are characterized by steep slopes with significant

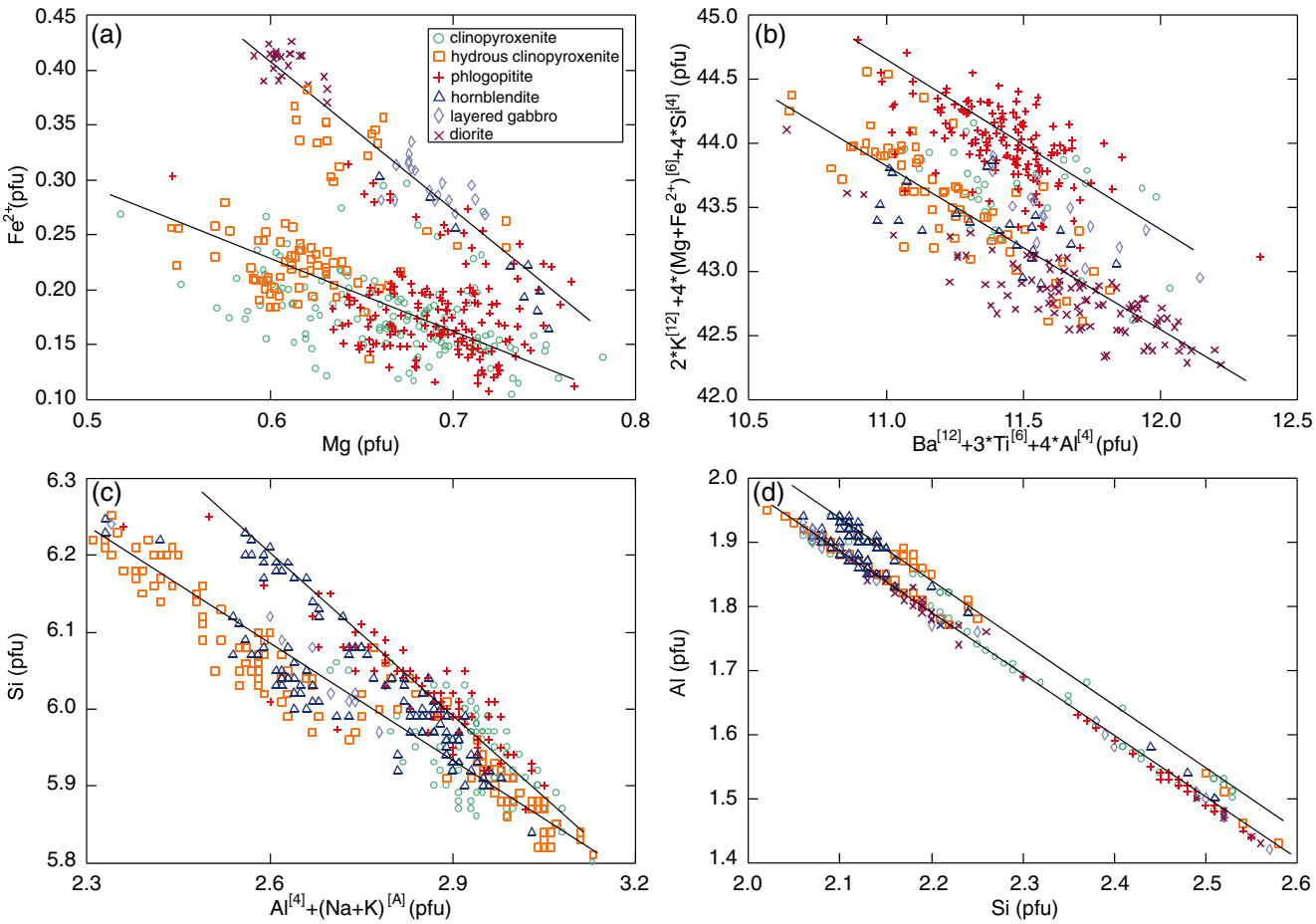

Fig. 4 Subtitutional mechanisms of the minerals displaying two distinct compositional trends: **a** clinopyroxene, **b** phlogopite, **c** pargasite, **d** plagioclase

Table 3 Ranges of geochemical data for each rock type. Whole data set is available upon request

Rocks	clinopyroxenite	phlogopitite	hydrous clinopyroxenite	hornblendite (fine grained)	hornblendite (coarse grained)	layered gabbro	Diorite
No. of samples	*14*	*9*	*20*	*1*	*7*	*1*	*1*
Elements							
SiO_2	45.3–48.8	43.6–46.79	40.3–48.7	42.5	38.4–42.3	46.1	43.5
TiO_2	0.68–1.15	1.02–1.62	0.57–2.09	1.56	1.45–2.97	0.34	2.3
Al_2O_3	6.14–9.10	8.04–10.5	8.5–19	14.7	14.3–18.7	26.7	17.1
Fe_2O_3	1.29–3.52	1.33–2.9	0.58–3.49	1.52	1.15–2.95	0.25	1.68
FeO	6.10–10.76	8.12–10.04	6.01–13.17	8.96	10.25–13.05	3.23	9.3
$FeO^{(t)}$	8.11–12.78	9.34–12.65	6.88–14.94	10.33	11.44–15.61	3.45	10.81
$Fe_2O_3^{(t)}$	9.01–14.2	10.37–14.05	7.65–16.6	11.47	12.72–17.35	3.84	12.01
MnO	0.14–0.23	0.17–0.2	0.14–0.24	0.17	0.15–0.5	0.07	0.16
MgO	9.14–11.94	11.98–12.87	4.45–11.32	12.03	7.17–9.09	3.08	6.55
CaO	18.4–22.5	13.38–18	10.45–20.84	13.59	11.47–14	16.84	11.93
Na_2O	0.47–1.01	0.46–0.75	0.75–1.57	1.83	1.26–1.54	1.4	0.73
K_2O	0.17–0.97	1.93–3.27	0.19–4.21	0.87	1.41–2.33	0.49	3.58
P_2O_5	0.04–0.68	0.03–0.4	0.03–0.9	0.03	0.02–0.5	0.05	0.88
Cr_2O_3	0.02–0.04	0.01–0.1	0.01–0.07	0.07	0.01–0.02	0.02	0.01
H_2O	0.75–1.08	1.11–1.73	0.78–2.35	1.47	1.49–2.48	0.7	1.49
CO_2	0.05–0.52	0.15–0.4	0.09–1.13	0.09	0.09–0.32	0.53	0.12
LOI	1.23–1.90	1.2–1.3	0.64–2.99		0.66–0.66		
Total	99.2–100.2	99.0–99.9	95.0–100.0	99.3	99.3–100.1	99.4	99.3
Mg#	0.62–0.75	0.68–0.73	0.44–0.72	0.71	0.55–0.60	0.63	0.56
$FeO^{(t)}$/MgO	0.70–1.31	0.76–1.04	0.88–1.90	0.86	1.43–1.72	1.12	1.65
Ba	44–827	1246–1644	96–2555	196	325–578	137	1695
Rb	7–41	56–99	5–107	7	19–27	–	138
Sr	125–278	118.2–183	212–847	299	320–515	837	391
Y	12–23.3	11.1–17	14–31	23	25–43	11	22
Zr	83–40	55.4–139	36–141	65	63–141	71	135
Nb	1.2–5.0	2.5–5.5	1.6–12		7.6–13	2.2	5
Th	1.1–3.4	0.8–2.1	0.52–4.4		1.5–5	2.9	2
Pb	3.9–16	4–14	4–19		17–96	20	10
Ga	11.0–14.2	11.1–14	13–19		19–21	19	22
Zn	29–89	41–83	42–138	50	79–110	26	115
Cu	15–60	20–100	15–111		32–69	14	52
Ni	16–79	18–38	14–112	147	10–23	16	10
V	276–528	280–607	124–697	452	516–716	179	357
Hf	3.7	2	2.7				
Cs	0.22–1.00	2.8–4.3	0.4–4.1		1.6–3.3	0.9	6.6
Sc	49–75	60–71	15–78	41	54–58	17	34
Ta	0.1–0.2	0.2–0.5	0.1–0.7		0.4–0.8	0.3	0.6
Co	34.2–38	46.7–69	33–58		48–53	17	44
U	0.4–1.1	0.3–0.7	0.17–1.4		0.4–0.9	1	0.7
Sn	1–1.9	1–1.6	1.1–4		1.1–1.9	0.4	0.9
Mo	4	1–2	3				
Cr	111–283	89–651	47–448	467	71–130	140	65
La	7.7–27.3	6.7–21	2–25	5.5	3–17	9.9	20
Ce	20–62.3	18.3–41	10–65	17	27–44	20	49
Pr	3.5–8.57	2.85–4.7	2.6–8.8	3.1	5–6.9	2.2	6.1
Nd	14–36.3	13.4–23	11–41	13	21–29	10	32
Sm	4–8.2	3.6–4.6	3.2–9.6	4.2	6.2–7.9	2.4	6.3
Eu	0.94–1.73	0.69–0.98	0.9–2	1.3	1.5–1.8	1.1	1.2
Gd	4–7.36	3.48–4.8	3.4–9.4	5	6.6–8.1	2.4	6.6
Tb	0.63–0.91	0.42–0.83	0.54–1.4	0.81	1–1.3	0.31	0.97
Dy	3.1–5.1	2.51–3.6	2.8–7.5	4.5	5.2–6.3	1.9	4.9
Ho	0.56–0.98	0.47–0.59	0.51–1.3	0.85	0.96–1.2	0.36	0.79

Table 3 (continued)

Rocks	clinopyroxenite	phlogopitite	hydrous clinopyroxenite	hornblendite (fine grained)	hornblendite (coarse grained)	layered gabbro	Diorite
No. of samples	*14*	*9*	*20*	*1*	*7*	*1*	*1*
Er	1.5–2.38	1.16–1.8	1.4–3.8	2.5	2.4–3.1	0.97	2.5
Tm	0.21–0.34	0.15–0.2	0.19–0.37	0.35	0.33–0.42	0.1	0.18
Yb	1.3–1.99	0.97–1.4	1.1–3.2	2.1	1.9–2.4	0.83	2
Lu	0.18–0.28	0.14–0.2	0.16–0.46	0.3	0.25–0.33	0.12	0.27
Nb/Y	0.09–0.24	0.18–0.34	0.11–0.39		0.30–0.42	0.20	0.23

enrichments in LILE and LREE relative to HFSE and HREE, respectively, and troughs at Nb-Ta, Zr-Hf and Ti.

Discussion

Physicochemical conditions

The estimates on physicochemical conditions give just an approach due to inappropriate mineral assemblages. Considering the limitations, the temperature is constraint to a range of 675–937°C for diopsidic augite and 750–930°C for pargasite (Toksoy-Köksal 2003). All temperature estimates approximate the amphibole liquidus temperatures in hydrous basaltic systems at low pressure (~900°C: Spear 1981). The pressure is restricted to a range of 5.83–16.45 kbar from diopsidic augite, 5–15 kbar from phlogopite, ~8.5–18 kbar from pargasite (Toksoy-Köksal 2003). The estimated pressure range of pargasite is higher than the other approximations probably due to exsolution of TiO_2 from pargasite to form Ti-phases (rutile and sphene) during slow cooling (Ernst and Liu 1998). Phlogopite bearing systems require high oxygen fugacity (Esperanca and Holloway 1987) and the studied phlogopite could only have formed at fO_2 conditions buffered between NNO and HM (Toksoy-Köksal 2003). Crystallization of high-An plagioclase also requires fO_2 to range between these buffers (Conrad et al. 1983).

Tectonic setting

The observed crystallization order of the minerals (clinopyroxene - phlogopite - pargasite I - plagioclase) is not typical for cumulates from continental (rift, arc) or oceanic (mid-ocean ridge, oceanic island, island arc) settings (for references see captions of Figs. 6 and 7).

The mineral assemblage of the Kurancali cumulates shows some similarity to those of island arc basements in the presence of hydrous phases. The assumed high water pressure and oxygen fugacity, LILE and LREE-enriched

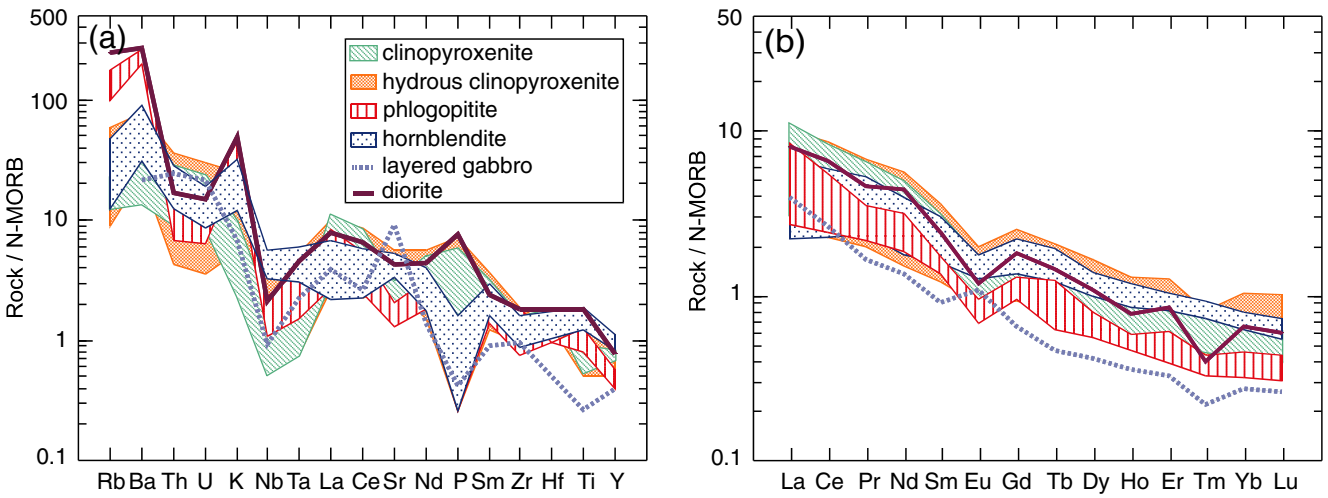

Fig. 5 N-MORB-normalized **a** spider and **b** REE patterns for the studied rocks (normalization data from Sun and McDonough 1989). The symbols in **b** are the same as those in **a**

patterns for clinopyroxenite, and high Ca-plagioclases also favor the generation of the cumulates above a subduction zone rather than in a rift-related system. The Kurancali rocks geochemically differ from cumulates of continental rifts, while they are comparable to those from roots of island arcs (e.g., V contents, negative Nb-Ta and Zr-Hf anomalies, high Pb abundances, and high ratios of Nb/Y and La/Yb) (e.g., Fig. 6). The attribution to continental arc is geochemically inadequate due to negative Zr-Hf anomalies of the studied rocks. In continental arc setting crustal contamination leads to positive Zr-Hf anomaly (e.g., Zhao and Zhou 2007).

Comparison of the mineral compositions with those of cumulates from different oceanic and continental settings (e.g., island arc, mid-oceanic ridge and oceanic island cumulates, and continental rift and arc cumulates, respectively) confirms the island-arc idea (for references see caption of Fig. 7). Clinopyroxene with higher Ca, Ti, Na,

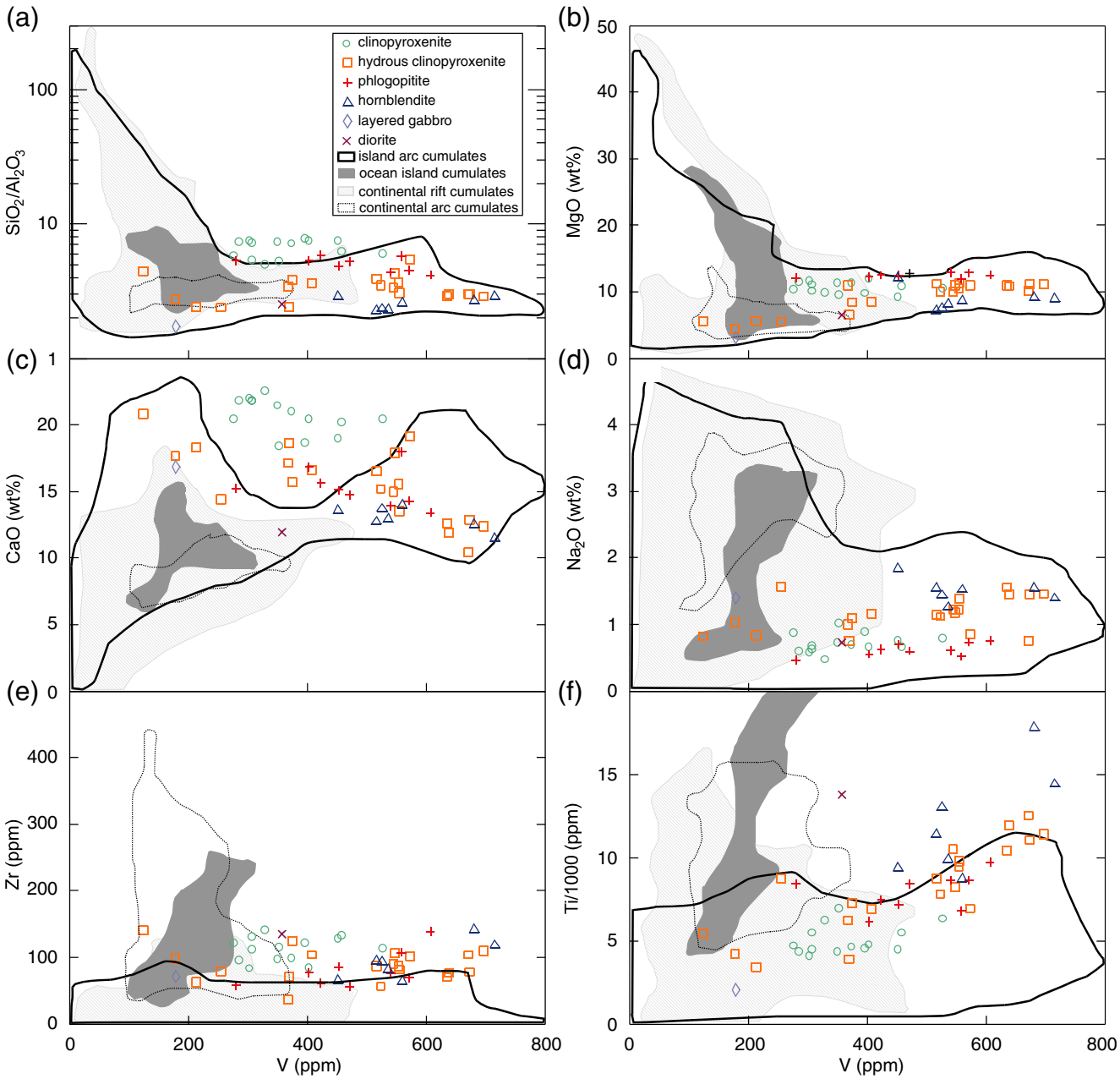

Fig. 6 Comparison of whole-rock geochemical data for the Kurancali cumulate rocks and cumulates from different settings (data compiled from Downes et al. 2001; Ait-Djafer et al. 2003; Dessai et al. 2004; Duchesne et al. 2004; Cawthorn and Boerst 2006; Maier et al. 2008 for continental rift cumulates; Duclaux et al. 2006; Marchev et al. 2006; Giacomini et al. 2007; Zhao and Zhou 2007 for continental arc cumulates; Himmelberg and Loney 1995; Béziat et al. 2000; Spandler et al. 2003; Dubois-Coté et al. 2005; Garrido et al. 2006; Greene et al. 2006; Krause et al. 2007; Takahashi et al. 2007 for island arc cumulates; Scoates et al. 2008 for oceanic island cumulates)

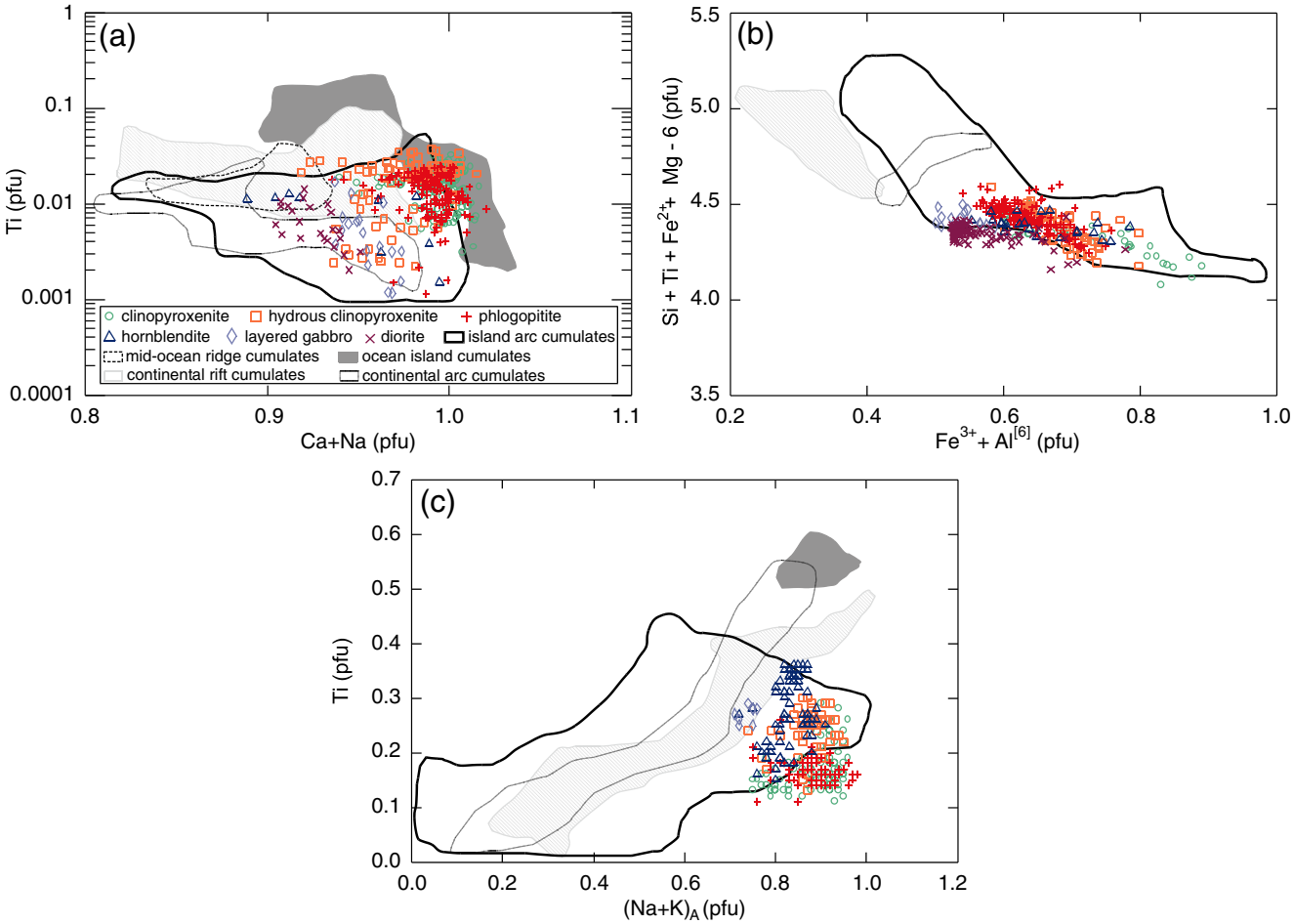

Fig. 7 Comparison between compositions of the minerals from the Kurancali cumulates and those from different settings where **a** diopisidic augite, **b** phlogopite, **c** pargasite (data compiled from Ait-Djafer et al. 2003; Dessai et al. 2004; Shaw 2004; Farahat et al. 2007 for continental rift cumulates; Marchev et al. 2006; Giacomini et al. 2007; Zhao and Zhou 2007; Tiepolo and Tribuzio 2008 for continental arc cumulates; Himmelberg and Loney 1995; Béziat et al. 2000; Spandler et al. 2003; Batanova et al. 2005; Farahat and Helmy 2006; Greene et al. 2006; Krause et al. 2007; Takahashi et al. 2007 for island arc cumulates; Tiepolo et al. 1997; Borghini et al. 2007 for mid-oceanic ridge cumulates; Alletti et al. 2005 for oceanic island cumulates)

$Al^{(t)}$, $Al^{[4]}$ (e.g., Fig. 7a), and phlogopite with lower Mg# and Na/(Na+K) values and higher Fe^{2+}, Fe^{3+}, $Al^{[6]}$ and Ti contents (e.g., Fig. 7b) are similar to those in island arc cumulates. Both pargasite I and II with high Ca-$Al^{(t)}$, Ti, Mg, Na and K contents, and high Na/K ratios are also comparable to the same (e.g., Fig. 7c).

The regional geological constraints (e.g., Göncüoglu et al. 1997) as well as geochemical evidence from the ophiolitic units (e.g., Yaliniz et al. 1996, 1999; Yaliniz and Göncüoglu 1998; Floyd et al. 2000; Kocak and Leake 1994; Kocak et al. 2005) favor the origin of the mafic cumulates in central Anatolia in a SSZ environment and exclude a continental arc as a possible origin as previously proposed (e.g., Kadioglu et al. 1998, 2003). Overall, geological, mineralogical and geochemical constraints imply that the Kurancali hydrous ultramafic-mafic cumulates are representative of an island arc basement formed during closure of the Neotethyan Izmir-Ankara-Erzincan branch of Neotethyan Ocean.

Magma and source character

Textural relations and compositional variations of the minerals in the Kurancali cumulates are typical of magmatic fractionation. Pargasite I and II, and phlogopite are of magmatic origin. High-Ti abundances of pargasite (0.96–2.61 wt.%) further support a primary origin of phlogopite since high-Ti pargasite has also high K_2O and a K-rich environment is required for it to occur in paragenesis with phlogopite. Chemical features of the minerals manifest crystallization from a magma with calc-alkaline to alkaline affinity. Despite its high $Al^{(t)}$ content the tetrahedral site of clinopyroxene is variably occupied by Si (1.71–1.99 pfu) with a negligible amount of $Al^{[4]}$ for some of analysed points. Clinopyroxene

in the ultramafic rocks has higher Na and K contents than that of the mafic ones. Moreover, phlogopite is OH- and Al-enriched, and Si-depleted. Tschermakitic exchange is predominant in pargasite I and II. Moreover, pargasite has high Ca-$Al^{(t)}$-Ti-Mg-Na-K contents, high Na/K ratios and extensive replacement of Si (5.80–6.27 pfu) by $Al^{[4]}$. Implications from mineral chemistry are confirmed by an increase of Na_2O, K_2O and Sr contents of the rocks with decreasing Mg#, and ascend of SiO_2 contents at nearly constant $FeO^{(t)}$/MgO ratios. Clinopyroxenite display calc-alkaline character, but the rest of the rocks show transition to alkaline nature as the amounts of hydrous phases increase.

Chemical features of the constituents, formation of phlogopite before pargasite, and late stage crystallization of plagioclase (Allan and Carmichael 1984), high-An plagioclase (e.g., Stern et al. 2006), and the absence of iron oxide minerals strongly infer crystallization from a highly water enriched melt. This hydrous magma might be derived from partial melting of a mantle source that was subjected to metasomatic event(s) above a subducted oceanic slab since hydrous metasomatising agents render partial melting of a mantle source easier to produce a hydrous melt (e.g., McInnes et al. 2001).

Cr and Ti contents of clinopyroxene are indicative of the magma-source character. The Cr content of clinopyroxene is much lower than that of clinopyroxene from MOR cumulates, and may reflect a depleted mantle source. The Ti content of clinopyroxene is highly variable from depleted to enriched values (Ti(pfu)*1000=0.37–35.93) compared to clinopyroxene in MOR cumulates. Lower Ti abundances support the idea of depletion of a mantle source by melting while higher values might be due to a Ti-rich agent metasomatically affecting this depleted source. In addition to Ti, enrichment of clinopyroxene in Ca, Na, $Al^{(t)}$ and $Al^{[4]}$ may be taken as evidence of metasomatism to have affected the depleted peridotitic mantle source. Low Fe^{3+}/$Fe^{(t)}$ ratio (0.22) and very high Ba contents of phlogopite and high Al, Ca, Na and K contents of pargasite may also be attributed to a metasomatised source. Additionally, accessory pyrite infers the presence of S in the system. Moreover, sporadic occurrence of apatite may require increase of CO_2/H_2O ratio in the melt after crystallization of hydrous phases such as amphibole and phlogopite (e.g., Zanetti et al. 1999).

Ratios between Zr, Nb, Ta, Yb, Ti, Zr and Y offer evidence about the character of the mantle source since these elements are potential markers of metasomatic effects in island arc magma sources (Green 1995). Zr/Y (1.71–10.8) and Zr/Nb (5.14–69.2) ratios are highly variable for the studied rocks (N-MORB=~2.9, ~30, respectively) that are intrpreted to represent depletion of a mantle source followed by metasomatic enrichment. Nb/Yb ratios of the rocks (0.92–5.42) are also higher than N-MORB (0.76). These high values cannot be explained by depletion of a mantle source because the Nb/Yb ratio of a melt decreases with depletion of the mantle source (Pearce et al. 2005). La/Yb ratios of the rocks (5.24–13.72) are much higher than N-MORB (~1.0) but this ratio should also decrease with increasing depletion in the source (e.g., Wang et al. 2001; Stern et al. 2006). The La/Yb ratios of the studied rocks are even higher than those of depleted mantle peridotites (e.g., Wang et al. 2001) and comparable to many cumulates from island arc basement (e.g., Spandler et al. 2003; Greene et al. 2006; Takahashi et al. 2007). It is evident that the Kurancali cumulates have crystallised from a melt derived from a lithospheric mantle which has been significantly modified by metasomatising components.

The hypothesis suggesting a metasomatised mantle source is also confirmed by similar enrichment levels in LILE, HFSE (especially Th, U, Zr) and LREE of clinopyroxenite and hornblendite. These enriched levels are consistent with the crystallisation of diopsidic augite from a melt derived from a metasomatised source to form the clinopyroxenites.

Implications on metasomatising agent(s)

The enrichment in LREE and LILE (e.g., Rb, Ba, Sr, K) resulting in high LILE/HFSE ratios, points to re-fertilization of a depleted mantle due to metasomatisation by subducting-slab-derived components in an island-arc setting. The components derived from dehydration of a subducting slab are highly variable and include hydrous fluids/melts (e.g., Plank and Langmuir 1993; Stern et al. 2006). The geochemical evidence from the Kurancali cumulates point to various different metasomatising agents. Elevated ratios of Rb/Sr (0.01–0.70), Ba/Th (35–1729), U/Th (0.18–0.53), Ba/La (7.1–197), Sr/Ce (4.12–41.9) and Ba/Rb (4.94–72.8) infer metasomatism of their mantle source by slab-derived hydrous fluids. LILE and other incompatible elements may have been derived from dehydration of subducted sediments (Plank and Langmuir 1993) or of oceanic crust (Ishikawa and Tera 1999). In sub-arc lithospheric mantle of an island arc, hydrous minerals can be formed as metasomatic minerals due to reaction of a peridotitic source with an initial low-density hydrous fluid having dissolved soluble major elements (Al, Ca, Na and K) (McInnes et al. 2001). Thus, metasomatism by alkali-rich hydrous fluids derived from early dehydration of a subducted slab may explain high Al, Ca, Na and K contents of the minerals and the rocks. However, enrichment of the rocks (including clinopyroxenite) in Nb, Ta, Yb, Ti, Zr, and Y relative to N-MORB (Sun and McDonough 1989) cannot be explained solely by infiltration with fluids, as these incompatible elements are not soluble and not mobile in hydrous fluids released by dehydration of a subducting oceanic slab

(Pearce and Peate 1995; Coltorti et al. 2007). However, melting of both subducted sediment and/or altered basaltic crust may produce siliceous melts contributing significant amounts of (e.g.) LREE, Th, Nb and Yb into mantle material (e.g., Defant and Drummond 1990; Elliott 2003; Green and Sinha 2005).

An adakitic melt (Defant and Drummond 1990) derived from subducted oceanic crust (e.g., Yogodzinski et al. 1995; Coltorti et al. 2007), which may metasomatise the mantle source, can partly explain highly varying ratios such as Zr/Hf (28–31), Ti/Eu (1853–12164) and Nb/Ta (7.3–24) not matching those of N-MORB (36.1, 7451, 17.7, respectively, Sun and McDonough 1989). Especially high Nb/Ta, Zr/Hf and La/Yb ratios of the rocks and their enrichment in incompatibles can be explained by adakitic melt metasomatism as this melt is characterized by strongly fractionated REE patterns with appreciable amounts of HFSE. High Zr/Hf and low Ti/Eu, Nb/Ta ratios of the rocks, on the other hand, can be interpreted as a result of carbonatite metasomatism (e.g., Ionov and Hoffman 1995; Gorring and Kay 2000). The amphibole, phlogopite, rutile and ilmenite-bearing mineralogy of the studied cumulates also favors a Fe-Ti-K-rich basaltic melt as a metasomatising agent in the mantle source area (e.g., Menzies et al. 1987). This may explain similar to or lower Zr/Hf ratios of the rocks compared to N-MORB, and their Ti/Eu ratios being similar to or higher than those of N-MORB. There is no further evidence of metasomatism by carbonatitic or basaltic components. However, Fe-Ti oxides, apatite, zircon and sphene of the studied rocks may require an adakitic melt as a metasomatising agent, since adakite-metasomatised mantle rocks have been demonstrated to contain these minerals (Prouteau et al. 2000). Silica-rich adakitic melts may also contain high H_2O and minor CO_2 (e.g., Andersen et al. 1993). Melting of an adakite-metasomatised source, therefore, will produce a hydrous magma with a composition suitable to crystallize the above-mentioned mineral assemblages. Adakitic melt may have been derived from wet melting of a hydrous oceanic crust (garnet-amphibolite or basaltic eclogite; e.g., Rapp et al. 1999, melting experiments at 3.8 GPa). Melting of eclogite with different clinopyroxene/garnet ratios in the residuum controls the positive or negative Zr anomalies in a liquid (Pertermann et al. 2004) and form SiO_2-Na_2O-Al_2O_3-rich melts (e.g., Kamchatka: Kepezhinskas et al. 1995; Aleutians: Yogodzinski et al. 1995; Styrian Basin, Austria: Coltorti et al. 2007). The interaction of this melt with depleted mantle wedge material results in crystallization of metasomatic pargasite and phlogopite (Sekine and Wyllie 1982; Sen and Dunn 1995), and in high Zr/Hf and Nb/Ta ratios (Ionov and Hoffman 1995). In this study, the metasomatising agent in the source was more likely to be an adakitic melt. It is interpreted to be responsible for the enrichment in SiO_2, Na_2O, K_2O, CaO and Al_2O_3 in hydrous melt derived from this source.

Trace and rare earth element abundances of the studied rocks are comparable to high-Al basalts with adakitic affinity (Toksoy-Köksal 2003). Their major and minor element concentrations, on the other hand, do not compare to them. They have lower SiO_2, FeO, Na_2O and K_2O concentrations and higher CaO and MgO concentrations (resulting in higher Mg#) than high-Al basalts. They may be interpreted as products resulting from interaction of a mantle wedge peridotite and a metasomatic melt derived from a subducting slab. Although, trace element contents of the slab melt were not modified significantly by this interaction, its major element composition seem to be modified. Experimental studies showed that small amounts of adakitic melt (i.e., peridotite:adakitic melt ratio=1:1) are entirely consumed in reaction with the host peridotite to form metasomatised zones (Sen and Dunn 1995; Rapp et al. 1999).

In addition to the principal metasomatic agent(s), the source(s) of magmatic water has to be identified. Phlogopite and pargasite in the Kurancali cumulates require high proportions of magmatic water for their crystallization. Moreover, the presence of primary hydrous mafic minerals (e.g., McInness et al. 2001), and the late crystallization of high-Ca plagioclase (e.g., Allan and Carmichael 1984) require significant amounts of water in the magma source. Water released from sediments and altered oceanic crust may not be sufficient to result in water contents as high as inferred for the magma that formed the Kurancali rocks. Serpentinized mantle is an alternative source of water to explain the high water content of the initial magma. In an intra-oceanic subduction zone, shallow lithospheric mantle may partly be serpentinized by water seeped from faults at the outer trench (Ranero et al. 2003) and by fluids originated from subducted oceanic crust and sediments (Peacock and Hyndman 1999). H_2O stored in serpentinites (~12 wt.%) can be subducted to greater depths than H_2O stored in altered MORB or sediments (Schmidt and Poli 1998). Serpentinite may dehydrate and release water (Yamasaki and Seno 2003) at ~150–250 km depth (Rüpke et al. 2004).

Implications on hybridisation

Hydrous cumulates contain less SiO_2 than clinopyroxenites, i.e. as the rocks become more evolved and more hydrous, their SiO_2 contents decrease. However, calc-alkaline cumulate rocks (e.g., from Aleutian arc, Alaska: Kay et al. 1990; Beaunit - French Massif Central: Féménias et al. 2003) show enrichment in SiO_2 as differentiation proceeds. Moreover, CaO behaves similar to SiO_2 and rises with increasing Mg# from hornblendite to clinopyroxenite. K_2O

and Na_2O contents, on the other hand, decrease with increasing Mg#. These constituents of the Kurancali cumulates oppose fractionation, and may indicate a complex possibly open system affected by a hydrous alkaline melt, i.e., hybridisation. Moreover, crystallization of phlogopite prior to pargasite supports this idea, as this cannot result from simple fractionation. Hybridisation is also verified by non-systematic variation of An content of plagioclase (41–99) and almost constant $Fe_2O_3^{(t)}$ content of plagioclase in all ultramafic rocks, and two distinct compositional trends recorded for clinopyroxene, phlogopite, pargasite I and plagioclase (e.g., Table 2, Fig. 4).

In addition, very high Nb/Yb (0.92–5.42), Zr/Yb (31.0–99.3) and Ti/Yb (2267–8653) ratios of the rocks (N-MORB=0.76, 24.3 and 2492, respectively) may indicate contributions from an incompatible element enriched alkaline melt. La/Sm and TiO_2/Al_2O_3 ratios, MgO content, and multi-element and REE patterns of the studied rocks are comparable with hornblendite cumulates of an alkaline melt from La Palma, the Canary Islands (Neumann et al. 2000). Arguing based on these ratios, the enrichment in HFSE was likely caused by hybridising alkaline melt. A hybrid parental magma, produced by mixing of a melt derived from partial melting of hydrous mantle wedge with an alkaline melt, may be responsible for the generation of the hydrous silica-undersaturated aluminous rocks. This might have led to crystallization of amphibole, phlogopite and clinopyroxene instead of orthopyroxene, resulting in selective enrichment in Rb, Ba, K and other elements compatible in these phases, as well as a general enrichment in incompatible elements with relative depletions in Nb, Ta, P and Ti.

A simple model on metasomatism and hybridisation

As discussed above, the studied rocks show a wide range in element ratios and high modal abundances of high-Ti pargasite-phlogopite±rutile±ilmenite±sphene. These features are interpreted to be the result of more than one metasomatic event in the magma source and hybridisation of the parental magma derived from this metasomatised source with alkaline melt. The data requires at least two types of metasomatic agents to have affected the depleted lithospheric mantle; dehydration from subducted slab probably caused enrichment in LILE, while an adakitic melt derived from melting of MORB-type oceanic crust probably resulted in Th, U, Zr, Hf and LREE-enriched in the magma and finally in the clinopyroxenite formed from it. Moreover, a hydrous alkali-basaltic melt leading to progressive enrichment in LILE and Nb (and Ta) in hornblendite is the hybridising component. In addition to hornblendite, the other investigated cumulate rocks are characterized by Nb-depletion (relative to elements with similar incompatibility) despite of their enrichment compared to MORB. Multiple metasomatic agents and hybridisation may explain the complexities in chemistry of the minerals and the rocks. If this was the case, it would require an explanation of how the metasomatising and hybridising agents evolved from low-Nb slab-derived adakitic melts to high-Nb alkaline melts, and what the source of the hybridising basaltic alkaline melt was.

Conclusions

The cumulate body from the Kurancali area in central Anatolia, found as an allochthonous isolated body on a metamorphic ophiolitic mélange, is characterized by the presence of (in the order of crystallization): clinopyroxene, phlogopite, pargasite and plagioclase. The rocks contain accessory Ti phases (sphene, rutile, ilmenite), pyrite and apatite. A lack of olivine and orthopyroxene is a characteristic feature of the body. Based on partitioning of Mg and Fe^{2+} among coexisting ferromagnesian minerals, in accordance with petrographic observations, the order of crystallization for the rocks was derived to be: clinopyroxenite - phlogopitite - hydrous clinopyroxenite - hornblendite - layered gabbro – diorite. The rocks and their constituents have the characteristic features of mantle origin but they display some unusual chemical compositions. Geochemical evidence infers that the rocks are generated in an island arc setting. Geothermobarometric estimates suggest that the rocks are representative of deep crust, probably in an arc basement.

All evidence from field, petrographical and geochemical studies on minerals and whole-rocks infers crystallization of the cumulates from a hydrous magma with high-K calc-alkaline affinity with slightly alkaline character under high water pressure and high oxygen fugacity conditions. Evidence from mineral and whole-rock geochemistry brings about that the melt must have been derived from a hydrous metasomatised mantle source above a subducted slab which was selectively enriched in LILE by a slab-derived fluid and an adakitic melt. The evidence also favors hybridisation of this hydrous magma with an alkaline melt to obtain hydrous silica-undersaturated aluminous rocks.

The metasomatising component(s) that modified the composition of the mantle wedge must have been H_2O-, alkali- and carbonate-rich aluminosilicate fluids/melts. The processes responsible for the crystallisation of phlogopite and pargasite at shallow levels in island arc basement, and the nature of metasomatising agent(s) affecting the mantle source, as well as hybridisation of alkaline and hydrous melt are still matters of debate. Further trace element and isotope geochemistry studies are necessary to decipher the origin, mechanism and quantity of the metasomatising

agent(s) (e.g., subduction derived fluid/melt) and the hybridisation of the dominant melt with alkaline liquid, as well as the source of water in the mantle (dehydration of subducting serpentinite?).

We suggest that the metasomatic agents in the subarc mantle led to the generation of the hydrous magma(s) that produced the Kurancali cumulates in an intra-oceanic subduction zone during the closure of the Izmir-Ankara-Erzincan branch of the Alpine Neotethys Ocean.

Acknowledgements This paper is a re-evaluation of the first author's PhD thesis. The author expresses her thanks to the German Academic Exchange Service (DAAD) and The Scientific and Technological Research Council of Turkey (TUBITAK) for the research grants to support her to complete part of the research in Potsdam University, Germany. The authors would like thank two anonymous reviewers for useful reviews of the manuscript and H. Marschall for editorial handling.

References

Ait-Djafer S, Ouzegane K, Paul-Liégeois J, Kienast JR (2003) An example of post-collisional mafic magmatism: the gabbro–anorthosite layered complex from the Tin Zebane area (western Hoggar, Algeria). J African Earth Sci 37:313–330

Allan JF, Carmichael ISE (1984) Lamprophyric lavas in the Colima graben, SW Mexico. Contrib Mineral Petrol 88:203–216

Alletti M, Pompilio M, Rotolo SG (2005) Mafic and ultramafic enclaves in Ustica Island lavas: Inferences oncomposition of lower crust and deep magmatic processes. Lithos 84:151–167

Andersen T, Austrheim H, Burke EAJ, Elvevold S (1993) N_2 and CO_2 in deep crustal fluids: evidence from the Caledonides of Norway. Chem Geol 108:113–132

Batanova VG, Pertse AN, Kamenetsk VS, Ariskin AA, Mochalo AG, Sobolev AV (2005) Crustal Evolution of Island-Arc Ultramafic Magma: Galmoenan Pyroxenite–Dunite Plutonic Complex, Koryak Highland (Far East Russia). J Petrol 46:1345–1366

Béziat D, Bourges F, Debat P, Lompo M, Martin F, Tollon F (2000) A Paleoproterozoic ultramafic-mafic assemblage and associated volcanic rocks of the Boromo greenstone belt: fractionates originating from island-arc volcanic activity in the West African craton. Precamb Res 101:25–47

Borghini G, Rampone E, Crispini L, De Ferrari R, Godard M (2007) Origin and emplacement of ultramafic–mafic intrusions in the Erro-Tobbio mantle peridotite (Ligurian Alps, Italy). Lithos 94:210–229

Boztug D, Tichomirowa M, Bombach K (2007) ^{207}Pb–^{206}Pb single-zircon evaporation ages of some granitoid rocks reveal continent-oceanic island arc collision during the Cretaceous geodynamic evolution of the central Anatolian crust, Turkey. J Asian Earth Sci 31:71–86

Cawthorn RG, Boerst K (2006) Origin of the Pegmatitic Pyroxenite in the Merensky Unit, Bushveld Complex, South Africa. J Petrol 47:1509–1530

Chalot-Prat F, Boullier AM (1997) Metasomatism in the subcontinental mantle beneath the Eastern Carpathians Romania: new evidence from trace element geochemistry. Contrib Mineral Petrol 129:284–307

Coltorti M, Bonadiman C, Faccini B, Ntaflos T, Siena F (2007) Slab melt and intraplate metasomatism in Kapfenstein mantle xenoliths (Styrian Basin, Austria). Lithos 94:66–89

Conrad WK, Kay SM, Kay RW (1983) Magma mixing in Aleutian arc: Evidence from cognate inclusions and composite xenoliths. J Volcan Geothermal Res 18:279–295

Defant MJ, Drummond MS (1990) Derivation of some modern arc magmas by melting of young subducted lithosphere. Nature 347:662–665

Dessai AG, Markwick A, Vaselli O, Downes H (2004) Granulite and pyroxenite xenoliths from the Deccan Trap: insight into the nature and composition of the lower lithosphere beneath cratonic India. Lithos 78:263–290

Downes H, Upton BGJ, Handisyde E, Thirlwall MF (2001) Geochemistry of mafic and ultramafic xenoliths from Fidra (Southern Uplands, Scotland): implications for lithospheric processes in Permo-Carboniferous times. Lithos 58:105–124

Droop GTR (1987) A general equation for estimating Fe^{3+} concentrations in ferromagnesian silicates and oxides from microprobe analysis, using stoichiometric criteria. Min Mag 51:431–437

Dubois-Coté V, Hébert R, Dupuis C, Wang CS, Li YL, Dostal J (2005) Petrological and geochemical evidence for the origin of the Yarlung Zangbo ophiolites, southern Tibet. Chemical Geology 214:265–286

Duchesne J-C, Liégeois J-P, Deblond A, Tack L (2004) Petrogenesis of the Kabanga–Musongati layered mafic–ultramafic intrusions in Burundi (Kibaran Belt): geochemical, Sr–Nd isotopic constraints and Cr–Ni behaviour. J African Earth Sci 39:133–145

Duclaux G, Ménot RP, Guillot S, Agbossoumondé Y, Hilairet N (2006) The mafic layered complex of the Kaby′e massif (north Togo and north Benin): Evidence of a Pan-African granulitic continental arc root. Precamb Res 151:101–118

Elliott T (2003) Tracers of the slab. In: Eiler J (ed) Inside the subduction factory, vol 138. American Geophysical Union, Geophysical Monograph, Washington DC, pp 23–45

Ernst WG, Liu J (1998) Experimental phase-equilibrium study of Al- and Ti-contents of calcic amphibole in MORB: A semiquantitative barometer. Am Mineral 83:952–969

Esperanca S, Holloway JR (1987) On the origin of some mica lamprophyres: experimental evidence from a mafic minette. Contrib Mineral Petrol 95:207–216

Farahat ES, Helmy HM (2006) Abu Hamamid Neoproterozoic Alaskan-type complex, south Eastern Desert, Egypt. J African Earth Sci 45:187–197

Farahat ES, Shaaban MM, Abdel Aal AY (2007) Mafic xenoliths from Egyptian Tertiary basalts and their petrogenetic implications. Gondwana Res 11:516–528

Féménias O, Coussaert N, Bingen B, Mercier J-CC, Demaiffe D (2003) A Permian underplating event in late- to post-orogenic tectonic setting. Evidence from the mafic-ultramafic layered xenoliths from Beaunit (French Massif Central). Chem Geol 199:293–315

Floyd PA, Göncüoglu MC, Winchester JA, Yaliniz MK (2000) Geochemical character and tectonic environment of Neotethyan ophiolitic fragments and metabasites in the Central Anatolian Crystalline Complex, Turkey. In: Bozkurt E, Winchester JA, Piper JDA (eds), Tectonics and Magmatism in Turkey and the Surrounding Area. Geol Soc Spec Publ London 173: pp 183–202

Garrido CJ, Bodinier J-L, Burg J, Zeilinger G, Hussain SS, Dawood D, Chaudhry MN, Gervilla F (2006) Petrogenesis of Mafic Garnet Granulite in the Lower Crust of the Kohistan Paleo-arc Complex (Northern Pakistan): Implications for Intra-crustal Differentiation of Island Arcs and Generation of Continental Crust. J Petrol 47:1873–1914

Giacomini F, Tiepolo M, Dallai L, Ghezzo C (2007) On the onset and evolution of the Ross-orogeny magmatism in North Victoria Land - Antarctica. Chem Geol 240:103–128

Gorring ML, Kay SM (2000) Carbonatite metasomatized peridotite xenoliths from southern Patagonia: implications for lithospheric processes and Neogene plateau magmatism. Contrib Mineral Petrol 140:55–72

Göncüoglu MC (1986) Geochronological data from the southern part (Nigde Area) of the Central Anatolian Massif. Bull Mineral Res Expl Ins, Turkey 105/106:83–96

Göncüoglu MC, Dirik K, Kozlu H (1997) Pre-Alpine and Alpine terranes in Turkey: Explanatory notes to the terrane map of Turkey. Annetes Geologiques des Pays Helléniques 37:515–536

Göncüoglu MC, Toprak GMV, Kuscu I, Erler A, Olgun E (1991) Geology of the western part of the Central Anatolian Massif: part II southern part. Unpublished Report No: 2909, Turkish Petroleum Company (in Turkish)

Green TH (1995) Significance of Na/Ta as an indicator of geochemical processes in the crust-mantle system. Chem Geol 120:347–359

Green NL, Sinha AK (2005) Consequences of varied slab age and thermal structure on enrichment processes in the sub-arc mantle of the northern Cascadia subduction system. J Volcan Geothermal Res 140:107–132

Greene AR, Debari SM, Kelemen PB, Blusztajn J, Clift PD (2006) A detailed geochemical study of island arc crust: the Talkeetna arc section, South–Central Alaska. J Petrol 47:1051–1093

Himmelberg GR, Loney RA (1995) Characteristics and Petrogenesis of Alaskan-Type Ultramafic-Mafic Intrusions, Southeastern Alaska. U.S. Geol Surv Professional Paper 1564:1–47

Ionov DA, Hoffman AW (1995) Nb-Ta rich mantle amphiboles and micas: implications for subduction related metasomatic trace element fractionations. Earth Planet Sci Lett 131:341–356

Ishikawa T, Tera F (1999) Two isotopically distinct fluid components involved in the Mariana arc: Evidence from Nb/B ratios and B, Sr, Nd, and Pb isotope systematics. Geology 27:83–86

Kadioglu YK, Ates A, Gülec N (1998) Structural interpretation of gabbroic rocks in Agacören Granitoid, central Turkey: field observations and aeromagnetic data. Geol Mag 135:245–254

Kadioglu YK, Dilek Y, Gülec N, Foland KA (2003) Tectonomagmatic evolution of bimodal plutons in the Central Anatolian Crystalline Complex, Turkey. Geol J 111:671–690

Kay SM, Kay RW, Perfit MR (1990) Calc-alkaline plutonism in the intra-oceanic Aleutian arc, Alaska. In: Kay SM, Rapela CW (eds), Plutonism from Antarctica to Alaska. Geol Soc Am Spec Paper 241: pp 233–255

Kepezhinskas PK, Defant MJ, Drummond MS (1995) Na-metasomatism in the island-arc mantle by slab melt-peridotite interaction: evidence from mantle xenoliths in the North Kamchatka Arc. J Petrol 36:1505–1527

Kocak K, Leake BE (1994) The petrology of the Ortaköy district and its ophiolite at the western edge of the Middle Anatolian Massif, Turkey. J African Earth Sci 18:163–174

Kocak K, Isık F, Arslan M, Zedef V (2005) Petrological and source region characteristics of ophiolitic hornblende gabbros from the Aksaray and Kayseri regions, central Anatolian crystalline complex, Turkey. J Asian Earth Sci 25:883–891

Köksal S, Göncüoglu MC (2008) Sr and Nd isotopic characteristics of some S-, I- and A-type granitoids from Central Anatolia. Turk J Earth Sci 17:111–127

Köksal S, Romer RL, Göncüoglu MC, Toksoy-Köksal F (2004) Timing of post-collisional H-type to A-type granitic magmatism: U-Pb titanite ages from Alpine Central Anatolian Granitoids (Turkey). Int J Earth Sci 93:974–989

Krause J, Brügmann GE, Pushkarev EV (2007) Accessory and rock forming minerals monitoring the evolution of zoned mafic–ultramafic complexes in the Central Ural Mountains. Lithos 95:19–42

Leake BE, Woolley AR, Arps CES, Birch WD, Gilbert MC, Grice JD, Hawthorne FC, Kato A, Kisch HJ, Krivovichev VG, Linthout K, Larid J, Mandarino JA, Maresch WV, Nickel EH, Rock NMS, Schmacher JC, Smith DC, Stephenson NCN, Ungaretti L, Whittaker EJW, Youzhi G (1997) Nomenclature of amphiboles: report of the subcommittee on amphiboles of the International Mineralogical Association, Commission on New Minerals and Mineral Names. Am Mineral 82:1019–1037

Maier WD, Barnes S-J, Bandyayera D, Livesey T, Li C, Ripley E (2008) Early Kibaran rift-related mafic–ultramafic magmatism in western Tanzania and Burundi: Petrogenesis and ore potential of the Kapalagulu and Musongati layered intrusions. Lithos 101:24–53

Marchev P, Arai S, Vaselli O (2006) Cumulate xenoliths in Oligocene alkaline basaltic and lamprophric dikes from the eastern Rhodopes, Bulgaria: Evidence for the existence of layered plutons under metamorphic core complex. Geol Soc Am Spec Paper 409:237–258

McInnes BIA, Grégoire M, Binns RA, Herzig PM, Hannington MD (2001) Hydrous metasomatism of the New Ireland Arc mantle xenoliths: Part 1. Petrology and geochemistry of fluid-metasomatised peridotites. Earth Planet Sci Lett 188:169–183

Menzies MA, Rodgers N, Tindle A, Hawkesworth CJ (1987) Metasomatic and enrichment processes in lithospheric peridotites, and effect of asthenosphere-lithosphere interaction. In: Menzies M, Hawkesworth CJ (eds) Mantle Metasomatism. Academic Press, London, pp 313–361

Morimoto N (1989) Nomenclature of pyroxenes. Can Mineral 27:143–156

Neumann E-R, Sorensen VB, Simonsen SL, Johnsen K (2000) Gabbroic xenoliths from La Palma, Tenerife and Lanzarote, Canary Islands: evidence for reactions between mafic alkaline Canary Islands melts and old oceanic crust. J Volcan Geothermal Res 103:313–342

Peacock SM, Hyndman RD (1999) Hydrous minerals in the mantle wedge and the maximum depth of subduction thrust earthquakes. Geophys Res Lett 26:2517–2520

Pearce JA, Peate DW (1995) Tectonic implications of composition of volcanic arc magmas. Annual Review of Earth Planetary Science 23:251–285

Pearce JA, Kempton PD, Nowell GM, Noble SR (1999) Hf–Nd element and isotope perspective on the nature and provenance of mantle and subduction components in western Pacific arc–basin systems. J Petrol 40:1579–1611

Pearce JA, Stern RJ, Bloomer SH, Fryer P (2005) Geochemical mapping of the Mariana arc-basin system: implications for the nature and distribution of subduction components. Geochem Geophys Geosyst 6(7). DOI 10.1029/2004GC000895

Pertermann M, Hirschmann MM, Kametner K, Günther D, Schmidt MW (2004) Experimental determination of trace element partitioning between garnet and silica-rich liquid during anhydrous partial melting of MORB-like eclogite. Geochem Geophys Geosyst 5:1–23

Plank T, Langmuir CH (1993) Tracing trace elements from sediment input to volcanic output at subduction zones. Nature 362:739–743

Prouteau G, Maury RC, Sajona FG, Cotton J, Joron JL (2000) Behaviour of niobium, tantalum and other high field strength elements in adakites and related lavas from the Philippines. The Island Arc 9:487–498

Ranero CR, Morgan JP, McIntosh K, Reichert C (2003) Bending related faulting and mantle serpentinization at the Middle America trench. Nature 425:367–373

Rapp RP, Shimizu N, Norman MD, Applegate GS (1999) Reaction between slab melts and peridotite in the mantle wedge: experimental constraints at 3.8 GPa. Chem Geol 160:335–356

Rieder M, Cavazzini G, D'Yakonov YS, Frank-Kamenetskii VA, Gottardi G, Guggenheim S, Koval PV, Müller G, Neiva AMR, Radoslovich EW, Robert J-L, Sassi FP, Takeda H, Weiss Z, Wones DR (1998) Nomenclature of the micas. Can Mineral 36:905–912

Rüpke LH, Phipps-Morgan J, Hort M, Connolly JAD (2004) Serpentine and the subduction zone water cycle. Earth Planet Sci Lett 223:17–34

Schmidt MW, Poli S (1998) Experimentally based water budgets for dehydrating slabs and consequences for arc magma generation. Earth Planet Sci Lett 163:361–379

Scoates Js, Weis D, Franssens M, Mattielli N, Annell H, Frey Fa, Nicolaysen K, Giret A (2008) The Val Gabbro plutonic puite: A sub-volcanic intrusion emplaced at the end of flood basalt volcanism on the Kerguelen Archipelago. J Petrol 49:79–105

Sekine T, Wyllie PJ (1982) Phase relationships in the system $KAlSiO_4$ - Mg_2SiO_4 - SiO_2 - H_2O as a model for hybridisation between hydrous siliceous melts and peridotite. Contrib Mineral Petrol 79:368–374

Sen C, Dunn T (1995) Experimental modal metasomatism of a spinel lherzolite and the production of amphibole-bearing peridotite. Contrib Mineral Petrol, 119, 422–432

Sengör AMC, Yilmaz Y (1981) Tethyan evolution of Turkey: a plate tectonic approach. Tectonophysics 75:81–241

Shaw SJ (2004) The temporal evolution of three magmatic systems in the West Eifel volcanic field, Germany. J Volcan Geothermal Res 131:213–240

Spandler CJ, Arculus RJ, Eggins SM, Mavrogenes JA, Price RC, Reay AJ (2003) Petrogenesis of the Greenhills Complex, Southland, New Zealand: Magmatic differentiation and cumulate formation at the roots of a Permian island-arc volcano. Contrib Mineral Petrol 144:703–721

Spear FS (1981) An experimental study of hornblende stability and compositional variability in amphibolite. Am J Sci 281:697–734

Stern RJ, Kohut E, Bloomer SH, Leybourne M, Fouch M, Vervoort J (2006) Subduction factory processes beneath the Guguan cross-chain, Mariana Arc: no role for sediments, are serpentinites important? Contrib Mineral Petrol 151:202–221

Sun SS, McDonough WF (1989) Chemical and isotopic systematics of ocean basalts: implication for mantle composition and processes. In: Saunders AD, Norry MJ (eds) Magmatism in Ocean Basins, Geol Soc London Spec Publ 42: pp 313–345

Takahashi Y, Mikoshiba MU, Takahashi Y, Kausar AB, Khan T, Kubo K (2007) Geochemical modelling of the Chilas Complex in the Kohistan Terrane, northern Pakistan. J Asian Earth Sci 29:336–349

Tiepolo M, Tribuzio R (2008) Petrology and U-Pb zircon geochronology of amphibole-rich cumulates with sanukitic affinity from Husky Ridge (NorthernVictoria Land, Antarctica): Insights into the role of amphibole in the petrogenesis of subduction-related magmas. J Petrol 49:937–970

Tiepolo M, Tribuzio R, Vannucci R (1997) Mg- and Fe-gabbroids from Northern Apennine ophiolites parental liquids and igneous differentiation processes. Ofioliti 22:57–69

Toksoy F (1998) Petrography and Mineralogy of the Vermiculitized Phlogopitic Metagabbro from the Kurancali Area (Kirsehir-Central Anatolia). Unpubl M.Sc. Thesis in Geological Engineering, Middle East Technical University, Ankara, 175 pp

Toksoy-Köksal F (2003) Petrology of the Phlogopite-Bearing Ultramafic-Mafic Plutonic Rocks within Central Anatolian Crystalline Complex, Turkey. Unpubl Ph.D. Thesis in Geological Engineering, Middle East Technical University, Ankara, 280 pp

Toksoy-Köksal F, Göncüoglu MC, Yaliniz MK (2001a) Petrology of the Kurancali Phlogopitic Metagabbro: An island arc-type ophiolitic sliver in the Central Anatolian Crystalline Complex, Turkey. Int Geol Rev 43:624–639

Toksoy-Köksal F, Türkmenoglu AG, Göncüoglu MC (2001b) Vermiculitization of phlogopite in metagabbro, central Turkey. Clays and Clay Minerals 49:81–91

Toksoy-Köksal F, Oberhaensli R, Göncüoglu MC (2007) Hydrous aluminosilicate metasomatism in an intra-oceanic subduction zone: Implications from the Kurancali ultramafic-mafic cumulates within the Alpine Neotethys Ocean, Turkey. Geochim Cosmochim Acta 71(15):A1026–A1026

Türeli TK, Göncüoglu MC, Akiman O (1993) The Petrology and origin of the Ekecikdağ granitoid (east of the Central Anatolian Crystalline Complex). Mineral Research and Exploration Institute (MTA) of Turkey Bulletin 115: 15–28 (in Turkish)

Wang ZH, Sun S, Hou QL, Li JL (2001) Effect of melt-rock interaction on geochemistry in the Kudi ophiolite (western Kunlun Mountains, northwestern China): implication for ophiolite origin. Earth Planet Sci Lett 191:33–48

Whitney DL, Teyssier C, Fayon AK, Hamilton MA, Heizler M (2003) Tectonic controls on metamorphism, partial melting, and intrusion: timing and duration of regional metamorphism and magmatism in the Nigde Massif, Turkey. Tectonophysics 376:37–60

Yaliniz MK, Göncüoglu MC (1998) General geological characteristics and distribution of the Central Anatolian Ophiolites. Hacettepe Üniversitesi Yerbilimleri Dergisi 20:19–30 (in Turkish)

Yaliniz MK, Aydın NS, Göncüoglu MC, Parlak O (1999) Terlemez quartz monzonite of Central Anatolia (Aksaray-Sarıkaraman): age, petrogenesis and geotectonic implications for ophiolite emplacement. Geol J 34:233–242

Yaliniz MK, Floyd PA, Göncüoglu MC (1996) Supra-subduction zone ophiolites of Central Anatolia: geochemical evidence from the Sarıkaraman Ophiolite, Aksaray, Turkey. Min Mag 60:697–10

Yaliniz MK, Göncüoglu MC, Özkan-Altiner S (2000) Formation and emplacement ages of the SSZ-type Neotethyan ophiolites in Central Anatolia, Turkey: palaeotectonic implications. Geol J 35:53–60

Yamasaki T, Seno T (2003) Double seismic zone and dehydration embrittlement of the subducting slab. J Geophys Res 108:2212 doi:10.1029/2002JB001918

Yogodzinski GM, Kay RW, Volynets ON, Loloskov AV, Kay SM (1995) Magnesian andesite in the western Aleutinian Komandorsky region; implications for slab melting and processes in the mantle wedge. Geol Soc Am Bull 107:505–519

Yu J-H, O'Reilly SY, Zhang M, Griffin WL, Xu X (2006) Roles of Melting and Metasomatism in the Formation of the Lithospheric Mantle beneath the Leizhou Peninsula, South China. J Petrol 47:355–383

Zanetti A, Mazzucchelli M, Rivalenti G, Vannucci R (1999) The Finero phlogopite-peridotite massif: an example of subduction-related metasomatism. Contrib Mineral Petrol 134:107–122

Zhao J-H, Zhou M-F (2007) Geochemistry of Neoproterozoic mafic intrusions in the Panzhihua district (Sichuan Province, SW China): Implications for subduction-related metasomatism in the upper mantle. Precambrian Research 152:27–47